Journal of Catalysis 282 (2011) 155–164

Contents lists available at ScienceDirect

Journal of Catalysis

journal homepage: www.elsevier.com/locate/jcat

Effect of water on the stability of Mo and CoMo hydrodeoxygenation catalysts: A combined experimental and DFT study

M. Badawi [a], J.F. Paul [a], S. Cristol [a], E. Payen [a], Y. Romero [b], F. Richard [b], S. Brunet [b], D. Lambert [c], X. Portier [d], A. Popov [e], E. Kondratieva [e], J.M. Goupil [e], J. El Fallah [e], J.P. Gilson [e], L. Mariey [e], A. Travert [e,*], F. Maugé [e]

[a] Unité de Catalyse et Chimie du Solide, Université de Sciences et Technologie de Lille, CNRS, 59650 Villeneuve d'Ascq, France
[b] Laboratoire de Catalyse en Chimie Organique, Université de Poitiers, CNRS, 40, avenue du Recteur Pineau, 86022 Poitiers, France
[c] Total Petrochemicals Research Feluy, Zone Industrielle C, B-7181 FELUY, Belgium
[d] CIMAP, ENSICAEN, Université de Caen, CNRS, CEA, 6, Boulevard du Maréchal Juin, 14050 Caen, France
[e] Laboratoire Catalyse et Spectrochimie, ENSICAEN, Université de Caen, CNRS, 6, Boulevard du Maréchal Juin, 14050 Caen, France

ARTICLE INFO

Article history:
Received 5 February 2011
Revised 23 May 2011
Accepted 5 June 2011
Available online 8 July 2011

Keywords:
Density functional theory (DFT)
Infrared spectroscopy
Carbon monoxide
HRTEM
Hydrodeoxygenation (HDO)
MoS_2
CoMoS
Water

ABSTRACT

We report the study of the impact of water on the stability of Mo and CoMo sulfide catalysts in hydrodeoxygenation of phenolic compounds. The presence of water at reaction temperature leads to an additional deactivation of the catalyst, which is fully reversible on the CoMo catalyst, but partly irreversible on non-promoted Mo catalyst. IR and HRTEM characterizations as well as DFT simulations confirm the higher sensitivity of unpromoted MoS_2 toward water and show that large amounts of water at reaction temperature lead to the exchange of an important fraction of edge sulfur atoms on non-promoted MoS_2 catalysts, hence changing the nature of the active sites. For Co-promoted catalyst, the extent of water poisoning is much lower and reversible because Co atoms prevent sulfur–oxygen exchanges. Hence, in HDO conditions, Co does not only increase the intrinsic activity of the catalyst (promotion effect) but also stabilizes the active phase in the presence of water (passivation effect).

1. Introduction

The European Union, the United States and many countries are promoting the use of non-edible lignocellulosic materials to produce biofuels to lower the consumption of fossil fuels and the emission of carbon dioxide without competing with a growing global demand for agricultural commodities [1]. Some green fuels, such as diesel, could be based on liquids derived from pyrolysis of lignocellulosic biomass. However, the bio-oil fraction produced by pyrolysis contains large amounts of oxygenated compounds (up to 45 wt.%) [2–4]. These molecules present multiple functions like aldehyde, ketone, acids and alcohols. High oxygen content leads to deleterious properties such as high viscosity, thermal and chemical instability as well as lower heating values than fossil sources [3–5]. The later was explained by the fact that combustion of oxygenated compounds is much less exothermic than that of hydrocarbons [6]. Hence, upgrading of bio-oils is mandatory to obtain usable fuels. Catalytic hydrodeoxygenation (HDO), a variant of hydroprocessing, refers to treatment of the feed under high temperature and hydrogen pressure to lower the oxygen content of the feedstock. Oxygen is removed as water or carbon oxides.

Sulfided hydrotreating catalysts such as $CoMo/Al_2O_3$ and $NiMo/Al_2O_3$ appear to be good candidates for HDO processing [3–10]. They are well-known catalysts and are extensively used in commercial hydrodesulfurization (HDS) and hydrodenitrogenation (HDN) processes; fundamental studies (in-depth experimental and theoretical investigations) greatly contributed to the understanding of their mode of action [7,11–18]. It is now well accepted that their active sites are located on the edges of MoS_2 nanocrystallites corresponding to the (1 0 0) edge planes of their layered structure [7,13,16]. This crystallographic (1 0 0) plane exhibits alternate rows of sulfur- (hereafter called S, or sulfur edge) and molybdenum-terminated layers (hereafter called M or molybdenum-edge) [13,16].

Lignocellulose is composed of cellulose (~40 wt.%), hemicellulose (~25 wt.%), lignin (~25 wt.%), extractives and inorganics (~10 wt.%). Lignin consists of aryl ether units connected by ether and alkyl bonds, and the cleavage of those bonds yields monomeric phenols and methoxyphenols [19]. Consequently, pyrolytic oils derived from such feedstocks contain a large amount of phenolic compounds, up to ~30% of the total oxygenated compounds

* Corresponding author.
E-mail address: arnaud.travert@ensicaen.fr (A. Travert).

0021-9517/$ - see front matter © 2011 Elsevier Inc. All rights reserved.
doi:10.1016/j.jcat.2011.06.006

[6,20,21]. Over sulfide-based catalyst, alkyl-phenols follow two main deoxygenation routes: one involves hydrogenation before C—O cleavage (HYD route) and the second one is a direct C—O bond cleavage (direct deoxygenation or DDO route) [22–31].

The stability of the sulfided catalysts in the presence of large amounts of oxygenated compounds and water is critical and may lead to modifications of the structure of the active edges of the sulfide phase [3,32]. Sulfided hydrotreating catalysts usually undergo a continuous deactivation caused by coke formation or partial reoxidation of the sulfide phase [3,4]. Water is known to have a slight inhibiting effect on the hydrodeoxygenation rate of phenolic compounds [23,33,34] or real feeds [35], which were related to a weak interaction between water and active sites at high temperature. Such an effect was also explained by the formation of a sulfate layer covering the active phase and reducing the catalytic activity [22]. However, water can also have a slight promoting effect in reactions such as HDN reactions [36].

The aim of the present study is to investigate the influence of water on the structure and activity of MoS_2-based sulfide catalysts using CO adsorption monitored by infrared spectroscopy (IR), high-resolution transmission electron microscopy (HRTEM), periodic density functional (DFT) calculations and catalytic activity measurements in HDO of 2-ethylphenol. Such a study will lead to a better understanding of sulfide catalysts and their active sites in working HDO conditions.

2. Materials and methods

2.1. Materials

The Mo/γ-Al_2O_3 and CoMo/γ-Al_2O_3 catalysts were prepared by conventional incipient wetness impregnation and supplied by TOTAL. Their chemical composition and textural properties are given in Table 1.

2.2. IR spectroscopy

For the infrared (IR) study, the catalysts were grounded and pressed into self-supported wafers. After introduction in a low temperature IR cell, sulfidation was carried out in situ under a flow of H_2S/H_2 (10/90) at 623 K during 2 h and followed by an evacuation during 1 h at the same temperature. CO was adsorbed on the sample cooled at 100 K. Small calibrated doses of CO were introduced in the IR cell up to an equilibrium pressure of 1 Torr. The sample was further evacuated from low temperature to 623 K. Subsequent water treatment (4.5 Torr of H_2O at equilibrium) was carried out at 623 K for 2 h and followed by evacuation at 623 K for 1 h. CO adsorption was repeated in the same conditions than previously described.

2.3. HRTEM analysis

Before HRTEM analysis, the catalysts were sulfided in the same conditions as for IR experiments. A fraction of the sulfided sample was contacted with water at 623 K during 16 h and followed by evacuation at 623 K for 1 h. A blank experiment was also done where the sulfided catalyst was heated (without water) in the closed cell at 623 K during 18 h and evacuated at 623 K for 1 h. After these various treatments, the samples were transferred under Ar in a glove box, gently crushed under Ar and stored under Ar before microscopic analysis. A drop of a suspension of the solid sample in *n*-butanol was deposited on a 300 mesh "holey carbon film" grid and dried at 298 K under argon flow before introducing in the high vacuum chamber of the microscope. HRTEM was performed on a JEOL 2010. The field emission gun was operated at 300 kV. For each sample, stacking degrees and lengths of ~1000 MoS_2 crystallites were measured.

Table 1
Chemical composition, BET surface area and pore volume of the catalysts.

	Mo/γ-Al_2O_3	CoMo/γ-Al_2O_3
BET area (m^2/g)	251	255
Pore volume (cm^3/g)	0.70	0.64
Mo (wt.%)	9.9	9.2
Co (wt.%)	–	4.2

2.4. Computational settings

The density functional theory (DFT) calculations were performed with the Vienna Ab initio Simulation Package (VASP) [37] using the generalized gradient corrections proposed by Perdew et al. [38]. The wavefunction is expanded in a plane wave basis set, and the electron–ion interactions are described using the projector augmented plane wave (PAW) method [39]. The solution of the Kohn–Sham equations was improved self-consistently until a difference lower than 10^{-5} eV was obtained between successive iterations. The calculations were performed with a cutoff energy of 450 eV and a Methfessel–Paxton smearing with $\sigma = 0.1$ eV. Throughout this work, we used the large super cell ($1.2641 \times 1.2294 \times 2.0000$ nm^3) shown in Fig. 1. It contains four elementary MoS_2 units in the *x* direction, four in the *z* direction and two layers along the *y*-axis. A *k*-point mesh (3, 1, 1) was chosen to give an accurate sampling of the Brillouin zone. A vacuum layer of 1 nm is located above the MoS_2 slab in the *z* direction in order to avoid interactions between slabs. The two upper rows were allowed to relax until forces acting on ions are smaller than 3×10^{-2} eV Å^{-1}. The two lower were kept fixed to simulate bulk constraints. Previous studies [16,17,40,41] showed that this model is suitable to predict the electronic and structural properties of the MoS_2 surface.

2.5. Thermodynamic treatment

Influence of the gas phase composition (H_2O vs. H_2S pressure) was taken into account by considering two reactions:

Adsorption of n H_2X species (X = O or S) on the surface:

$$\text{surface} + n\ H_2X = \text{surface} - H_{2n}X_n \quad (1)$$

and S—O exchange reaction:

$$\text{surface} - S_n + n\ H_2O = \text{surface} - O_n + n\ H_2S \quad (2)$$

Gibbs free energy of Reaction (2), for example, was computed according to:

$$\Delta_r G = \mu(\text{surface} - O_n) - \mu(\text{surface} - S_n) + n(\mu(H_2S) - \mu(H_2O))$$

Assuming that the difference between the chemical potential of solid phases can be approximated by the difference in their electronic energy [42] led to:

$$\Delta_r G = \Delta_r G^0 + n\ RT \ln 10 \log P(H_2S)/P(H_2)$$

where

$$\Delta_r G^0 = \Delta E_n + \Delta\mu^0(T)$$

and

$$\Delta E_n = E(\text{surface} - O_n) - E(\text{surface} - S_n) - n\ E(H_2O) + n\ E(H_2S)$$

ΔE_n being the electronic energy contribution to the S—O exchange reaction.

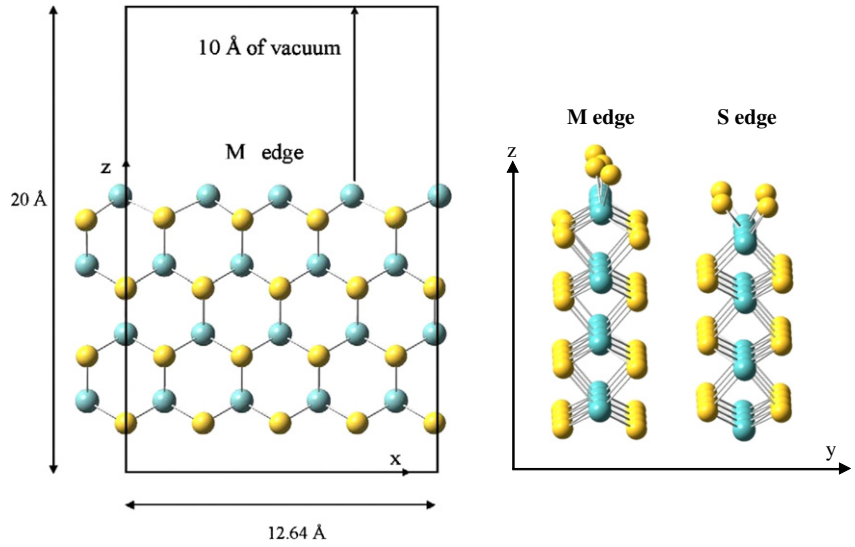

Fig. 1. On the left, cell showing the perfect MoS_2 (1 0 0) surface. On the right, cell showing the stable MoS_2 surface when $0.05 < H_2S/H_2 < 10{,}000$ [40,41] that will be used as reference. Molybdenum atoms are in blue, sulfur atoms are in yellow. (For interpretation of the references to color in this figure legend, the reader is referred to the web version of this article.)

The gas phase molecules chemical potentials $\mu^0(T)$ were computed according to statistical thermodynamic equations for ideal gas [42,43]. The most stable surface is then the one presenting the lowest Gibbs free energy. The calculations were performed at $T = 623$ K, which corresponds to the working temperature of the catalyst and H_2S/H_2O partial pressure ratios between 10^{-4} and 10^2.

2.6. Activity measurements

The particle size of the catalysts was in the range of 250–315 μm. The catalysts were diluted in carborundum to keep the volume of the catalyst bed constant. In order to obtain comparable conversions, 50 mg of promoted catalyst or 100 mg of unpromoted catalyst were used.

All the catalysts were sulfided in situ into a high-pressure dynamic flow reactor (length: 40 cm; inner diameter: 1.25 cm) using a mixture of 5.8 wt.% dimethyldisulfide (DMDS) in toluene, under 4.0 MPa of total pressure (Table 2). The sulfiding mixture was injected at a starting temperature of 423 K. After 1 h, the temperature was raised to 623 K at a rate of 5 K/min and it was maintained at this temperature for 14 h. The temperature was then lowered to the reaction temperature (613 K).

The catalytic test was carried out less than 7 MPa of total pressure using 2-ethylphenol (2-EtPh) as oxygenated model compound diluted in toluene. Its partial pressure was fixed to 49 kPa. DMDS was added to the feed to generate 30 kPa of H_2S during the reaction in order to preserve the sulfide state of the catalyst. The partial pressure of hydrogen was kept constant at 5.75 MPa by changing the partial pressure of the solvent (Table 2). Methylcyclohexane obtained from toluene hydrogenation was observed in very low quantities: less than 1 mol% whatever the contact time used.

The reactor effluents were condensed and liquid samples periodically collected and analyzed with a Varian 3300 chromatograph equipped with a DB1 capillary column (length: 30 m; inside diameter: 0.50 mm; film thickness: 0.25 μm) and a flame ionization detector. The oven temperature was programmed from 328 K (maintained for 5 min) to 448 K (4 K/min). The products were identified by using GC/MS analysis (Finnigan INCOS 500) and by co-injection of commercial samples provided by Aldrich. Gaseous products were not found except for methane, which was produced by DMDS decomposition.

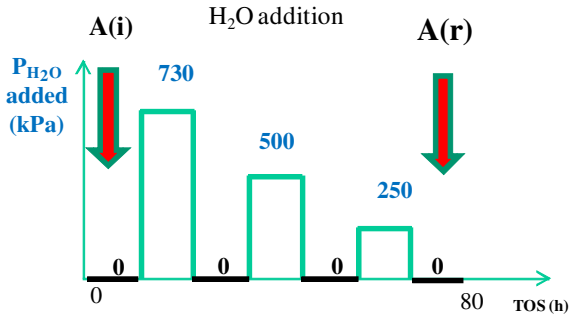

Fig. 2. Evolution of water partial pressure during 2-ethylphenol HDO reaction.

The model oxygenated feed and water were injected separately by using two pumps. Various model feeds were used in order to keep constant the partial pressures of 2-EtPh, H_2S and H_2.

The experimental procedure to study the impact of water addition on 2-EtPh deoxygenation is depicted in Fig. 2 and described later:

Step 1: Hydrodeoxygenation of 2-EtPh was carried out without water. Conversions were kept lower than 20% in order to measure the activity (A_i). The activities were measured after stabilization of the catalyst. Contact times of 1.04 min and 2.3 min were used for unpromoted and promoted catalysts, respectively.

Table 2
Partial pressures of the various compounds in sulfidation and reaction conditions.

	P_{total} (MPa)	P_{H_2} (MPa)	$P_{toluene}$ (MPa)	$P_{2\text{-EtPh}}$ (kPa)	P_{H_2S} (kPa)	P_{CH_4} (kPa)	P_{H_2O} (kPa)	H_2O/H_2S ratio
Sulfidation conditions	4	2.67	1.07	–	129	129	–	-
Reaction conditions	7	5.75	0.39–1.14	49	30	30	250–730	8.3–24.3

Step 2: Water was injected at in the feed for 8 h at various pressures (730, 500 and 250 kPa, successively).

After each step 2, step 1 conditions were reestablished for 6 h in order to quantify the degree of catalyst deactivation. The final HDO rate (A_f) was measured at the end of this procedure.

2.7. XPS and elemental analysis of spent catalysts

Chemical analysis of carbon and sulfur was carried out after testing and was obtained by using an elementary analyzer (NA2100 analyzer, CE instruments). Prior analysis, the catalysts were washed with dichloromethane during 24 h under reflux and dried at 110 °C for 24 h in order to remove physisorbed hydrocarbons.

For the XPS analysis, the reactor was cooled down after the reaction, flushed with argon and transferred in a glove box in order to avoid any air oxidation. XPS spectra were recorded using an Axis Ultra DLD system (Kratos Analytical – UK), monochromatic Al Kα X-ray radiation ($h\nu$ = 10,476 eV). The samples are analyzed at a 90° take-off angle, and the hydrocarbon component of the C 1s spectrum (285.0 eV) is used as calibration of the energy scale. Fitting of the XPS spectra is performed using CasaXPS processing software.

3. Results

3.1. IR study

Fig. S1 (Supplementary information) shows the IR spectra of CO adsorbed on Mo/Al_2O_3 and $CoMo/Al_2O_3$ sulfide catalysts after sulfidation. As described in previous studies [44,45], adsorption on the freshly sulfided catalysts leads to the appearance of bands at 2190 and 2155 cm^{-1} corresponding to CO interacting with Lewis acid sites (Al^{3+}) and acidic AlO—H groups of the uncovered alumina support. On the Mo/Al_2O_3 (Fig. S1A), a main band at 2110 cm^{-1} is detected that characterizes Mo edge sites of the sulfided MoS_2 slab. On the $CoMo/Al_2O_3$ catalyst in addition to this band, two bands at 2072 cm^{-1} and at 2055 cm^{-1} (shoulder) are observed (Fig. S1A). They correspond to promoted sites in various environments [44]. Addition of small doses of water over the sulfide catalysts at 298 K leads to a progressive poisoning of the acidic sites of the alumina support (spectra not shown). In these conditions, a subsequent adsorption of CO shows that water does not interact significantly with the sulfide phase sites. A decrease in the number of these sites is only observed when large amounts of water are in contact with the catalyst [46]. Hence, in mild conditions (small partial pressure of water at 295 K), water preferentially adsorbs on the oxide support than on the sulfide phase.

Table 3
Effect of the posttreatments with H_2O and H_2S on the variation of CO uptake on the various sulfided sites of (Co)Mo catalysts.

Catalysts	Mo/Al_2O_3	$CoMo/Al_2O_3$	
νCO frequency (cm^{-1})	2110	2110	2072, 2055
After water treatment at 623 K	−45%	−72%	−28%
After water treatment and resulfidation at 623 K	–	−54%	+6%

Adsorption of CO on Mo/Al_2O_3 and $CoMo/Al_2O_3$ sulfide catalysts after water treatment at high temperature leads to spectra showing similar bands as after sulfidation (Fig. S1), but with different intensities. Fig. 3 compares the spectra obtained before and after water treatment at 623 K on sulfided $(Co)Mo/Al_2O_3$ and shows that the CO uptake by the sulfide sites strongly decreases after water treatment. Such a decrease is observed for both Mo and CoMo catalysts. On the CoMo catalyst, water treatment has not the same impact on non-promoted Mo sites (2110 cm^{-1}) and promoted sites (2072–2055 cm^{-1}): the decrease in the intensity of the CO band characterizing the non-promoted Mo sites is significantly larger (−72 ± 14%) than that of promoted sites (−28 ± 7%), as shown in Table 3. An intermediate decrease is observed on the non-promoted Mo/Al_2O_3 catalyst (∼−45%).

In order to check the reversibility of the water poisoning, a resulfiding treatment was carried out on the CoMo catalyst under the same conditions as for the initial sulfidation (623 K, H_2S/H_2 10/90, 2 h). Fig. 3b and Table 3 clearly show that such a treatment leads to the complete regeneration of the promoted CoMoS sites, while the non-promoted sites are still strongly poisoned after resulfidation (−54%, Fig. 3 and Table 3).

Finally, IR and Raman analysis of the water treated samples did not reveal the presence of ν(Mo=O) bands, indicating that no oxidic entities (MoO_3 or oxomolybdate species) were formed after such a treatment.

3.2. HRTEM analysis

HRTEM micrographs of sulfided $(Co)Mo/Al_2O_3$ catalysts present black thread-like fringes as observed in previous HRTEM studies that correspond to the MoS_2 slabs [47,48]. An example of TEM image is presented in the Supplementary information (Fig. S2). After water treatment at 623 K, no major changes in the aspect and repartition of the sulfide slabs were noted. To compare quantitatively the distribution of slabs length and stacking before and after water treatment, statistical analyses were made based on the analysis of about 50 images and 1000 slabs located in various parts of

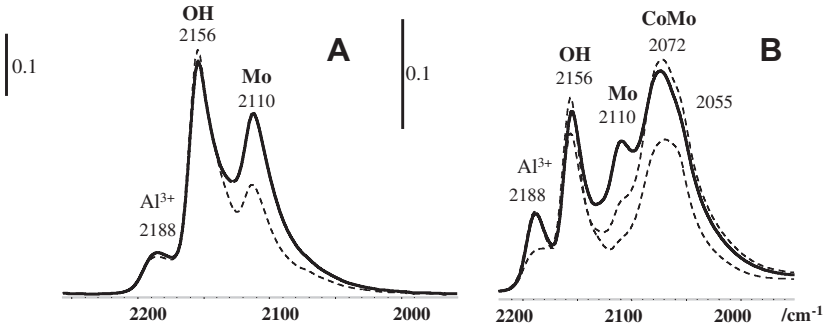

Fig. 3. IR spectra of CO adsorbed on sulfided catalysts after sulfidation (line), after water treatment at 623 K (dashed line), after resulfidation at 623 K (dotted dashed line) – A– Mo/Al_2O_3; B – $CoMo/Al_2O_3$.

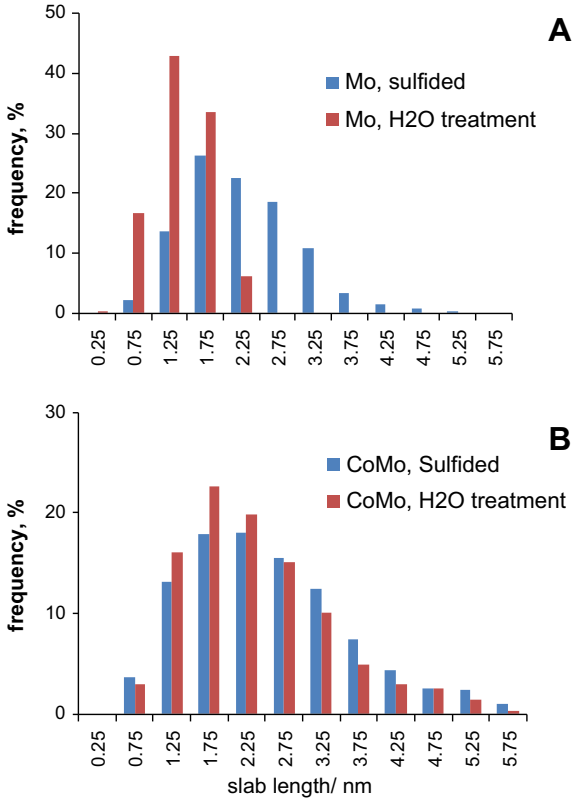

Fig. 4. HRTEM analysis of the effect of water treatment on the slab length of sulfided (Co)Mo/Al_2O_3 catalysts – A – Mo/Al_2O_3; B – CoMo/Al_2O_3 – blue bars: after sulfidation; red bars: after sulfidation and water treatment at 623 K. (For interpretation of the references to color in this figure legend, the reader is referred to the web version of this article.)

the same sample. The sulfide slab length and stacking distribution for Mo and CoMo catalysts are presented in Fig. 4 and Table 4.

After sulfidation and in the absence of water treatment, the average slab length of the sulfide slabs is close for Mo and CoMo catalysts (2.4 and 2.6 nm, respectively).

After water treatment of the sulfided Mo catalyst, the slabs length distribution is clearly shifted toward lower slab lengths, resulting in the decrease of the average slab length from 2.4 to 1.6 nm (Table 4). The average stacking is not significantly changed on this sample. In addition, no MoO_3 crystallites were detected after water treatment.

The size of the sulfide slabs of the CoMo catalyst appear much less affected by the water treatment: no effect on stacking can be detected from the change of the average values, whereas the average sulfide slab length decreases from 2.6 to 2.4 nm after water treatment. Although this difference is small, a chi-square (χ^2) test used to compare the length distribution before and after water treatment showed a statistically significant difference between both distributions ($p < 0.01$). In order to confirm the low sensitivity of CoMo catalysts to water, a HRTEM analysis of CoMo/Al_2O_3 catalyst was performed after the sulfidation procedure used in catalytic test as well as after HDO test of 2-ethylphenol (Table 4). Similar average slab length and stacking are measured before and after the HDO test.

In conclusion, although water treatment leads to a decrease in the average slab length for both catalysts, the non-promoted Mo/Al_2O_3 catalyst is much more sensitive to water than CoMo/Al_2O_3.

Table 4
Effect of water treatment on the average slab length (L) and stacking (n) of sulfided slabs of (Co)Mo/Al_2O_3.

Treatment	Mo/Al_2O_3		CoMo/Al_2O_3	
	L (nm)	n	L (nm)	n
Sulfidation by H_2S/H_2 at 623 K	2.4	1.4	2.6	1.0
Sulfidation by H_2S/H_2 at 623 K followed by water treatment at 623 K	1.6	1.1	2.4	1.1
Sulfidation by DMDS at 623 K	–	–	2.4	1.3
Sulfidation by DMDS at 623 K followed by standard HDO test	–	–	2.3	1.2

3.3. DFT calculations

3.3.1. Stability of the MoS_2 phase

The stability of non-promoted MoS_2 surfaces under typical hydrotreating conditions has been widely studied and reviewed in the last years [16–18,40,41,49]. In presence of H_2 and H_2S, the most stable surface [16,40,41], which will be used as reference, is presented in Fig. 1. The molybdenum-edge is covered with sulfur atoms, yielding sixfold coordinated Mo edge atoms [17,40]. Within the same partial pressure and temperature range, the sulfur edge is reduced: half-sulfur atoms are removed from the surface leading to fourfold coordinated molybdenum atoms.

Water can adsorb on unsaturated molybdenum sites of the surface or lead to sulfur–oxygen atom exchanges, hence strongly modifying the surface state. In a previous work [32], we investigated the effect of water on the stability of the two types of edges considering only sulfur–oxygen (S—O) exchanges. In the present study, we report in addition the adsorption of H_2S and H_2O on the molybdenum phase in order to get a more complete view of MoS_2 stability under HDO conditions.

On the M-edge (Table 5), neither adsorption of H_2O (or H_2S) nor S—O exchange lead to stable surfaces in the partial pressure range investigated in this study ($10^{-4} < P(H_2X) < 10^2$, with X = O or S). The M-edge is fully covered by S atoms, and Mo atoms remain sixfold coordinated.

On the opposite, the presence of water in the gas phase induces surface modification of the S-edge (Fig. 5). On this edge, H_2O and H_2S adsorption are dissociative and less endothermic as compared to the M-edge (Table 5). The values of H_2O and H_2S adsorption Gibbs free energies indicate that stable adsorption should occur under high partial pressure. Interestingly, H_2O adsorption is more difficult than H_2S adsorption on the S-edge. Finally, Gibbs free energy calculations demonstrate that exchange of the sulfur atoms located on the edge by oxygen atoms is possible for water partial

Table 5
MoS_2 ΔG^0 (eV) calculated at 350 °C (corresponding to the $\Delta E + \Delta\mu^0(T)$ term) for the three following reactions: (1) adsorption of n H_2O molecules, (2) adsorption of n H_2S molecules, (3) n S—O exchanges – the free energy reaction is divided by n.

Reaction	Number of reactions n	M-edge	S-edge
(1) H_2O adsorption	1	1.00 (molecular)	0.64 (dissociative)
	2	1.09 (molecular)	0.60 (dissociative)
(2) H_2S adsorption	1	1.29 (molecular)	0.25 (dissociative)
	2	1.44 (molecular)	0.20 (dissociative)
(3) S—O exchange	1	0.62	0.21
	2	0.55	0.24
	4	0.60	0.26

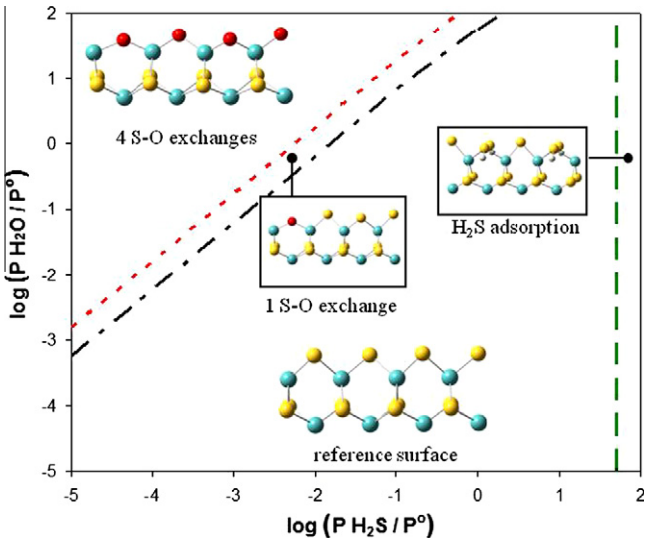

Fig. 5. Stability diagram of the thermodynamic stable surfaces of the MoS_2 S-edge under HDO conditions as a function of log ($P(H_2S)/P^0$) and log ($P(H_2O)/P^0$).

pressure greater than 40 times the H_2S partial pressure. It is worth noting that this exchange could occur even at low total H_2O/H_2S pressure.

Taking into account both reactions and thermodynamic corrections, the diagram shown Fig. 5 can be built, which shows that several types of surfaces are stable in the HDO conditions: the fully sulfided edge with fourfold coordinated molybdenum atoms (reference surface); at high H_2S partial pressure (log ($P(H_2S)/P^0$) > 1.7) and whatever H_2O partial pressure, H_2S dissociative adsorption is possible, leading to the formation of S—H groups on the surface; for lower H_2S partial pressures (log ($P(H_2S)/P^0$) < 1.7), the increase in H_2O partial pressure can lead to the exchanges of one (or more) sulfur atoms (one exchange for $P(H_2O)/P(H_2S) > 40$; full exchange for $P(H_2O)/P(H_2S) > 200$). These surfaces are then oxygenated, but the formal oxidation state and the coordination of the Mo atoms are kept constant.

The stability diagram (Fig. 5) shows that it is essential to keep a partial pressure in H_2S during the HDO process in order to avoid the desulfurization of the catalyst, which is consistent with experimental observations [27]. However, the amount of H_2S to be added in the feed need to be controlled otherwise, it leads to H_2S adsorption on the MoS_2 catalyst and will inhibit the HDO reactions [10,23,25].

3.3.2. CoMoS phases

The addition of promoter atoms such as cobalt or nickel on the catalyst increases its activity [7,12,31,50,51]. The evolution of the surface stochiometry as a function of the partial pressures in H_2O and H_2S will be the key parameter to improve our understanding of the reaction. Based on STM observations [52,53], it was proposed that the Co atoms are mostly localized on the S-edge. However, IR experiments [44,54] suggest that a part of the Co atoms, in the case of high Co/Mo ratio, is also located on the M-edge. According to DFT studies [17,53,55,56], the S-edge is supposed to be fully promoted, while the M-edge is only partially substituted. In order to be able to describe the experimental Co/Mo ratio, we performed a systematic study of the promoter effect on the surface stability in presence of water.

Similarly to the results described on the non-promoted system, the addition of water is not favored on the promoted surface (Table 6). This result is valid for both edges and for molecular or dissociative adsorptions. It can be noticed that adsorption energies are the most endothermic for the fully promoted edges.

Table 6
CoMo ΔG^0 (eV) calculated at 350 °C for the three following reactions: (1) adsorption of n H_2O molecules, (2) adsorption of n H_2S molecules.

Reaction	Promotion degree (%)	M-edge	S-edge
(1) H_2O adsorption	25	0.70 (dissociative)	0.35 (molecular)
	50	0.32 (molecular)	0.30 (molecular)
	100	0.50 (molecular)	1.28 (molecular)
(2) H_2S adsorption	25	0.95 (dissociative)	0.54 (dissociative)
	50	0.44 (molecular)	0.35 (dissociative)
	100	0.29 (molecular)	1.19 (dissociative)

Table 7
CoMoS ΔG^0 (eV) calculated at 350 °C for n S—O exchange reactions – the Gibbs free energy is divided by n.

Promotion degree	Number of reactions n	M-edge	S-edge
25%	1	0.68	0.12
	2	0.69	0.15
	4	0.72	0.37
50%	1	0.12 (top)	0.23
	2	0.13 (top)	0.31
	4	0.41 (basal)	0.37
100%	1	0.96	0.86
	2	0.90	0.81
	4	0.95	0.86

The S—O exchange energies are reported in Table 7. On the M-edge, the substitution of one Mo atom by one Co (25% promoted M-edge) leads to the formation of fivefold coordinated atoms as already mentioned [16,18], but the addition of water or the S—O exchange remains not favored. The same conclusion occurs for the fully promoted M-edge. On the opposite, the S—O exchange is possible on the 50% promoted M-edge as soon as $P(H_2O)/P(H_2S)$ is greater than 10 (Fig. 6). The terminal Mo—S bond is easily transformed in a Mo—O one in presence of water in the gas phase. However, this exchange does not change the coordination of the Co atom, which would be the adsorption site of the reactive molecules.

The results on the S-edge show that addition of promoter Co atoms will stabilize the sulfide phase, almost stable under HDO conditions. The presence of traces of sulfur in the feedstock should be enough to get a stable catalyst. Fig. 7 summarizes the calculations on the S-edge surface stability giving the number of exchanged atoms depending on the promotion degree and reaction conditions.

3.4. Hydrodeoxygenation of 2-ethyphenol

Some of us reported previously [31] that the 2-EtPh transformation over (Co)Mo/Al_2O_3 sulfided catalysts follows three pathways (Scheme 1). The first one called the hydrogenation route (HYD) leads to the production of 1-ethylcyclohexene, 3-ethylcyclohexene and ethylcyclohexane. The second route, the direct deoxygenation (DDO), leads to the formation of ethylbenzene. In the present experimental conditions, ethylbenzene is not hydrogenated into ethylcyclohexane, indicating that these two routes are parallel. A third pathway (ACI) which involves mainly the acidic sites of the

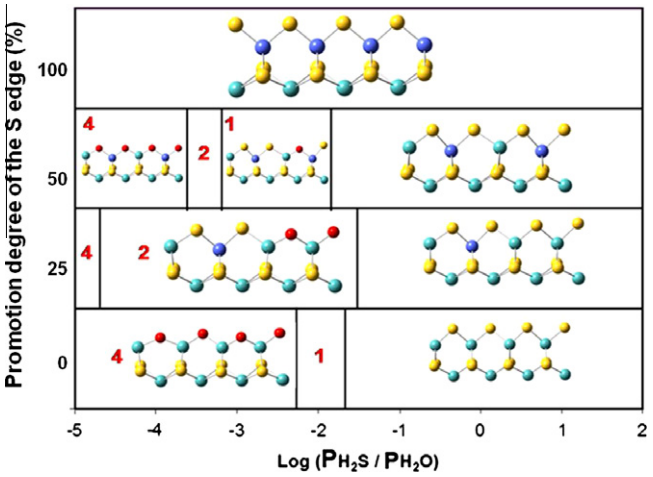

Fig. 6. Stability diagram of the thermodynamic stable surfaces of the M-edges of CoMoS and MoS_2 phases under HDO conditions – the number in red indicates the number of sulfur–oxygen exchanges as a function of the promotion degree and log ($P(H_2S)/P(H_2O)$). Color code: Co in dark blue, Mo in light blue, S in yellow, O in red. (For interpretation of the references to color in this figure legend, the reader is referred to the web version of this article.)

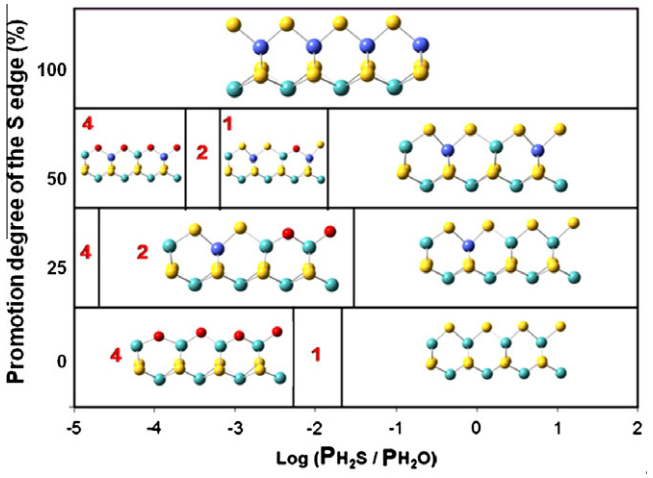

Fig. 7. Stability diagram of the thermodynamic stable surfaces of the S-edges of CoMoS and MoS_2 phases under HDO conditions – the number in red indicates the number of sulfur–oxygen exchanges as a function of the promotion degree and log ($P(H_2S)/P(H_2O)$). Color code: Co in dark blue, Mo in light, S in yellow, O in red. (For interpretation of the references to color in this figure legend, the reader is referred to the web version of this article.)

alumina support leads to the formation of oxygenated compounds by isomerization and disproportionation reactions (phenol, diethylphenols and 3-ethylphenol). These oxygenated compounds are further deoxygenated and produce benzene, cyclohexane, cyclohexene diethylbenzenes and diethylcyclohexanes.

In the presence of 30 kPa of H_2S in the feed (and in absence of added water - step 1 conditions), the Co-promoted sulfide catalyst is three times more active in deoxygenation than the unpromoted catalyst (Fig. 8a). In fact, both the activities for the HYD and DDO pathways are greater over the $CoMo/Al_2O_3$ (Fig. 8b–c) than over Mo/Al_2O_3 catalyst. The DDO activity is markedly improved in presence of cobalt. The DOD/HYD ratio increases from 0.26 for unpromoted catalyst to 0.85 for CoMo catalyst. In these conditions (step 1), the deoxygenated products represented about 80% of the total compounds over the CoMo catalyst and about 58% over the non-promoted catalyst. Consequently, the amount of water generated by the HDO reaction is 4.9 kPa for the unpromoted catalyst and 7.8 kPa for the promoted catalyst.

To determine the effect of water on the stability and selectivity of the sulfided catalysts, quantities of water (between 250 kPa and 730 kPa) larger than that formed during the HDO reaction were introduced on the catalyst (step 2 conditions). Thus, one can consider that the partial pressure of water is constant on the two catalysts irrespective of the time on stream. It should be mentioned that large amounts of water can be typically found during the HDO of bio-oils [4] and that the partial pressures used in the present study are in the range of those used in previous studies (see, e.g., [33,34]). The activity-time profiles for the HYD and DDO routes on the Mo catalyst are reported Fig. S2 in the Supplementary information. It clearly evidence a fast decrease in the HYD activity in the presence of water as well as a fast recovery (about as fast as the initial decrease), which is only partly reversible. Fig. 8a shows the effect of water addition on the steady-state HDO activity for Mo and CoMo catalysts. This causes a decrease in activity of the two catalysts. The activity drop is independent of the added water partial pressure. Over the unpromoted catalyst, the HDO activity (Fig. 8a) is reduced by about 2.2 times, whereas over the Co-promoted catalyst, the HDO activity is only decreased by a factor of 1.3.

The effect of water addition is different for the two 2-EtPh deoxygenation pathways. For unpromoted and promoted catalysts, the HYD pathway is most sensitive to water addition than the DDO route (Fig. 8b and c). Indeed, the HYD activity drops by a factor about 3 for the Mo catalyst and by a factor of 1.3 on the CoMo catalyst. By contrast, the DDO pathway appears almost insensitive to water addition on the two catalysts. Such a difference leads to a marked improvement of the DDO/HYD selectivity when water is added. The ratio is increased from 0.26 to 0.81 for the unpromoted catalyst and from 0.85 to 1.11 for the promoted catalyst. This improvement of the DDO over the HYD activity reduces the H_2 consumption with only a small penalty in overall HDO activity.

In the last step, the test conditions are set to their initial values in order to estimate the catalyst sensitivity to water addition. For the various routes, the activity ratios $(A_r)/(A_i)$ (A_r: residual activity, A_i: activity in step 1) are presented in Table 8. For the unpromoted catalyst, the initial HDO activity is not totally recovered. Indeed, for the Mo catalyst, the (A_r/A_i) ratio is equal to 0.75, mainly due to an irreversible loss of activity in the HYD route. In the absence of water, this ratio is 0.96 after the same time on stream (80 h), indicating a moderate deactivation in the absence of water, likely due to coke and/or water produced during the reaction. By contrast, over the Co-promoted catalyst, the (A_r/A_i) ratio is 0.91 for HDO vs. 0.93 after the same time on stream in absence of added water. The activities in both deoxygenation routes are equally recovered. These catalytic results show that the catalyst stability under a water cover is improved by the presence of the cobalt that also acts as promoter.

3.5. Chemical and XPS analysis of spent catalysts

Chemical analysis of sulfur was carried out on the Mo catalyst after catalytic testing for the same time on stream, in the presence or the absence of added water. The sulfur content was similar in both cases within the precision of the method (4.9 ± 0.2 wt.%).

Quasi in situ XPS analysis of Mo and CoMo catalysts was also carried out. The corresponding spectra are reported in Fig. S4 of the Supplementary information section and elemental surface composition from XPS is reported in Table 9. Fig. S4 shows that the Mo 3d XPS spectra of the spent catalysts with or without added water are nearly superimposable, indicating that no significant change of the Mo oxidation state occurs during the water treatment. Similarly, Table 9 indicates that no significant change in

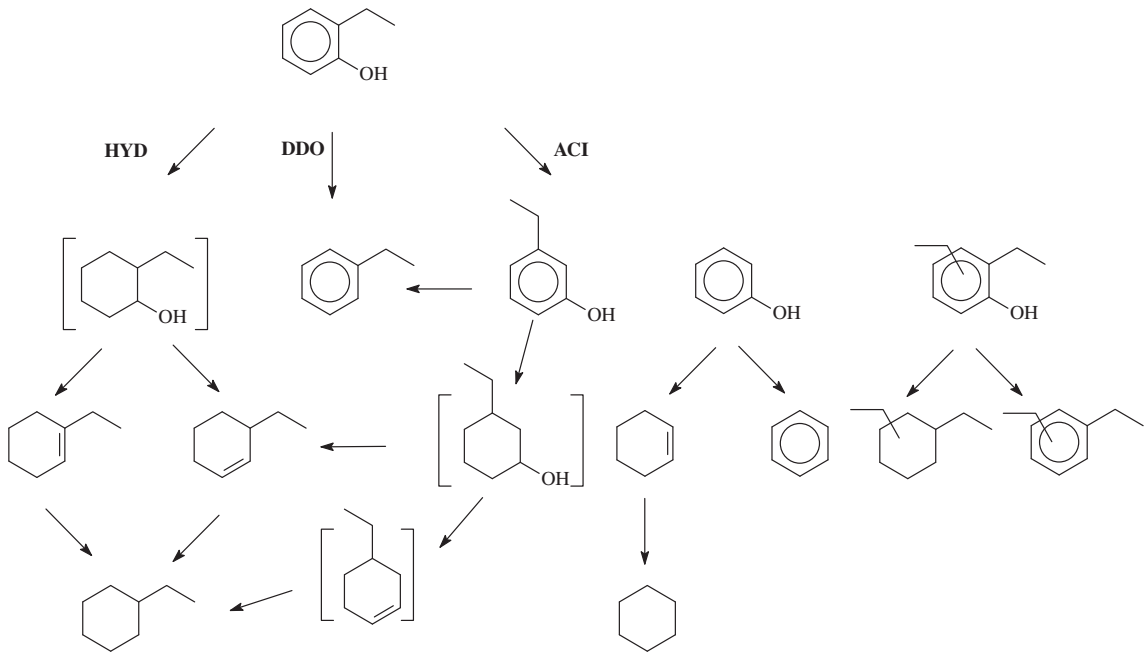

Scheme 1. Transformation of 2-ethylphenol over sulfided Mo-based catalysts.

the amount of sulfide molybdenum (Mo(IV)) and sulfur (S(-II)) occurs after the water treatment, within the uncertainty due to the deconvolution of the XPS spectra. Hence, no significant oxidation of the sulfide phase could be evidenced by any of the characterization techniques used in the present study (TEM, IR, Raman, XPS, elemental analysis).

4. Discussion

For both the Mo and CoMo catalysts, an inhibition upon H_2O addition is observed in the deoxygenation of 2-EtPh. Nevertheless, the Mo catalyst is much more sensitive to water addition than CoMo. The results also show that water affects much more the HYD than the DDO pathway. This strongly suggests that different types of active sites are involved in these two routes, as already proposed by several authors for deoxygenation of phenolic compounds [24,25]. Similar proposals were already proposed for HDS of dibenzothiophenic compounds, which are also desulfurized by two parallel ways (namely DDS and HYD routes) [57] and for HDN reactions [58].

The effect of water addition on the HDO activity is almost completely reversible on the CoMo catalyst, while the activity of the Mo sample is not fully recovered when water is removed. The question of the origin of the water effect arises. Several hypotheses can be proposed: (i) formation of an oxidic phase, (ii) sintering or demixion of the sulfide phase, (iii) poisoning of the active sites by water and (iv) S—O exchanges of the outer layer of the sulfide slabs.

The multitechnique characterization of the catalysts of this study will allow discriminating between these proposals.

4.1. Formation of an oxidic phase

Under reaction conditions, the H_2 partial pressure is always very high (Table 2). Thus, even in the presence of added water, an oxidation of the metallic atoms of the catalyst is thermodynamically unlikely. Furthermore, IR and Raman spectroscopies of the water treated samples do not reveal the presence of any oxidic entities (MoO_3 or oxomolybdate entities), in agreement with HRTEM analysis of the sulfide catalysts after water treatment, although the latter is not very sensitive to the presence of oxysulfide phases [48]. However, as indicated by the quasi in situ XPS analysis of the spent catalysts after testing with or without added water, no formation of a significant fraction of oxysulfide phase under the HDO conditions with added water was evidenced.

4.2. Sintering or demixion of the CoMoS phase

HRTEM observations show a decrease in the sulfide slab size after water treatment on Mo and CoMo catalyst (Table 4). Therefore, sintering of the sulfide particles cannot be considered to account for the water effect. For the CoMo catalyst, this conclusion is confirmed by the total reversibility of the water effect on the HDO activity (Table 8) as well as on the IR spectra of CO adsorbed on the CoMoS phase (Table 3). These experimental observations also prove that cobalt demixion from the CoMoS phase does not occur significantly in presence of water.

4.3. Poisoning of the active sites by water

IR monitoring of CO adsorption indicates that, at 298 K, water strongly interacts with the alumina support whereas it does not much affect the sulfide sites. On the unpromoted catalyst, DFT calculations show that H_2O is only weakly adsorbed on the preferentially exposed M-edge of MoS_2. Moreover, CO adsorption energy on this edge is much higher than that of H_2O (0.5–0.6 eV vs. 0.2 eV). Hence, molecularly adsorbed water – if any – would be displaced by CO. Although adsorption energies of H_2O and CO are similar on the S-edge (~0.7 eV), it is difficult to draw any clear conclusion from the experimental spectra because CO adsorption on S-edge sites is difficult to quantify from the IR spectra [45]. Similar conclusions can be drawn from DFT calculations of the adsorption energy of water and CO on promoted system (−0.85 eV and −1.59 eV, respectively, for the 50% promoted M-edge). These finding are in good agreement with our experimental results showing that on sulfided catalysts (Mo/Al_2O_3 and $CoMo/Al_2O_3$), water in the gas phase hardly competes for adsorption sites on the sulfide phase as already observed by Laurent and Delmon [25].

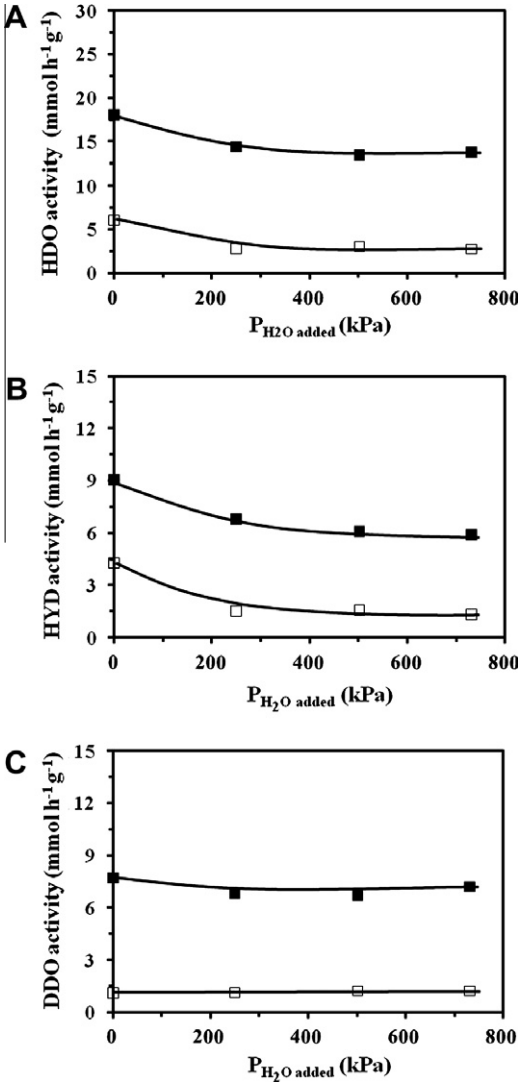

Fig. 8. Transformation of 2-ethylphenol over sulfide catalyst at 613 K less than 7 MPa of total pressure. Effect of water addition on the catalyst activity. $CoMo/Al_2O_3$ (solid symbols), Mo/Al_2O_3 (empty symbols). HDO activity (A); HYD activity (B), and DDO activity (C).

Table 8
Effect of water addition on the catalytic stability of sulfided (Co)Mo/Al_2O_3 for the different routes of EtPh HDO.

	A_r/A_i	
	Mo/Al_2O_3	$CoMo/Al_2O_3$
HDO	0.75 (0.96)[a]	0.91 (0.93)[a]
HYD	0.73 (0.96)[a]	0.90 (0.93)[a]
DDO	0.91 (0.96)[a]	0.92 (0.93)[a]

[a] In bracket: relative activity after the same time on stream in the absence of water.

4.4. S—O exchanges of the outer layer of the sulfide slabs

DFT calculations show that a sulfur–oxygen exchange is possible on the outer layer of the sulfide slabs (Figs. 5–7). This exchange certainly modifies the electronic properties of the edge sites of the sulfide slabs and may be at the origin of the water effect experimentally observed by different techniques. Furthermore, our calculations point out that this exchange is easier on the non-promoted edges than on the promoted ones whatever the degree of promotion. In the same way, the experimental data (IR, HRTEM and activity tests) demonstrate the greater water sensitivity of the unpromoted sulfided phase.

Table 9
Surface composition of spent catalysts tested with or without added water derived from XPS spectra.

Catalyst	Condition	Mo(IV)/Al	S(-II)/Al
Mo/Al_2O_3	Without H_2O	0.027	0.074
	With H_2O	0.021	0.089
$CoMo/Al_2O_3$	Without H_2O	0.025	0.117
	With H_2O	0.027	0.095

Table 10
Evolution of the Mo—Mo computed distances (in Å) due to the S—O exchange.

	Parallel to the edge	Perpendicular to the edge
MoS_2 without exchange	3.05 and 3.25 alternatively	3.09 ± 0.02
MoS_2 partial exchange	Between 2.92 and 3.41	3.10 ± 0.10
MoS_2 full exchange	Between 3.08 and 3.52	3.10 ± 0.12

The particle size decrease after water treatment (HRTEM) is compatible with the formation of an oxy-sulfide outer layer. Indeed, the exchange of sulfur by an oxygen atom on the edges leads to a structural distortion and a crystallinity loss of the external layer of sulfide slabs. Table 10 shows the Mo—Mo distances in non-exchanged and oxygen exchanged MoS_2 model surfaces. These data clearly confirm that sulfur–oxygen exchange leads to significant changes of Mo—Mo distances. This effect can be accounted by the strong differences in Mo—O and Mo—S average bond lengths (0.19 and 0.23 nm, respectively). Such a distortion would lead to the absence of diffraction fringes from the outer Mo layer of the MoS_2 sulfide slabs. Consequently, this could explain why the sulfide particles appear smaller in HRTEM. Taking into account the Mo—Mo distance in crystalline MoS_2 (0.316 nm), the exchange of edge sulfur atoms by oxygen should lead to a decrease of ~0.6–0.7 nm of the slab length as observed by HRTEM. These values are very close to the decrease of 0.8 nm of the average slab length observed on the Mo/Al_2O_3 catalyst after water treatment. The absence of a large decrease in the slab length on $CoMo/Al_2O_3$ is explained by the presence of Co atoms on the MoS_2 slab edges, which (i) does not contribute to the diffraction pattern and (ii) limits the extent of S—O exchanges.

The strong decrease in CO uptake by unpromoted catalyst observed after water treatment can be explained by a decrease in the number of edge sulfide sites induced by S—O exchange. Computed adsorption energy of CO on the M-edge of MoS_2 decreases from 0.6 eV on the non-exchanged surface to 0.1 eV on the fully O-exchanged M-edge. Such a decrease can be explained by the larger electronegativity of the oxygen with respect to sulfur, which lowers the extent of back-donation of Mo d electrons in the π^* CO orbital.

5. Conclusion

Several techniques were used to understand the impact of water on the stability of Mo and CoMo sulfide catalysts supported on alumina. The main findings can be summarized as follows:

(i) Water addition during the hydrodeoxygenation of 2-ethylphenol decreases slightly the catalyst activity. This is fully reversible on the CoMo catalyst, but partly irreversible on the unpromoted Mo catalyst.

(ii) IR characterization highlights that a water treatment at reaction temperature leads to a strong and irreversible decrease in the number of unpromoted Mo sites, while the poisoning of the Co-promoted sites occurs to a lower extent and is fully reversible.
(iii) HRTEM demonstrates that a water treatment at reaction temperature leads to a strong decrease in the average length of crystalline MoS_2 slabs of the unpromoted catalyst (−0.8 nm), while this length is almost unchanged on the promoted CoMo catalyst.
(iv) DFT calculations show that incorporation of cobalt at the edge of the MoS_2 sulfide phase increases its stability toward water.

All these findings indicate that on unpromoted MoS_2 catalysts, the presence of large amounts of water at reaction temperature can lead to the exchange of a large fraction of edge sulfur atoms, hence changing the nature of MoS_2 edge sites. For Co-promoted catalyst, the extent of water poisoning is much lower and reversible because Co atoms prevent sulfur–oxygen exchanges. Hence, in HDO, Co does not only increase the intrinsic activity of the catalyst (promotion effect) but also stabilizes active phase in the presence of water (passivation effect).

Acknowledgments

This work is funded by the French ANR *Programme National de Recherche sur les Bioénergies* – ECOHDOC, a joint project between the Centre National de la Recherche Scientifique (CNRS), the universities of Caen, Lille and Poitiers and TOTAL. We acknowledge the USTL Centre de Ressources Informatiques (partially funded by FEDER) for allocating CPU time. We thank A. Beaurain and M. Trenteseaux for the XPS analysis.

Appendix A. Supplementary data

Supplementary data associated with this article can be found, in the online version, at doi:10.1016/j.jcat.2011.06.006.

References

[1] (a) Off. J. Eur. Union L140 (2009) 88;
(b) J. Earley, A. McKeown, Red, White and Green: Transforming US Biofuels, Worldwatch Institute, Washington, DC, 2009.
[2] (a) A.V. Bridgwater, G.V.C. Peacocke, Sustain. Energy Rev. 4 (2000) 1;
(b) G.X. Huber, S. Iborra, A. Corma, Chem. Rev. 106 (2006) 4044.
[3] E. Furimsky, Appl. Catal. A: Gen. 199 (2000) 147.
[4] D.C. Elliott, Energy Fuels 21 (2007) 1792–1815.
[5] S. Czernik, A.V. Bridgwater, Energy Fuels 18 (2004) 590.
[6] M.N. Islam, R. Zailani, F.N. Ani, Renew. Energy 17 (1999) 73.
[7] H. Topsøe, B.S. Clausen, F.E. Massoth, Hydrotreating Catalysts: Science and Technology, Springer, Germany, 1996. pp. 22, 141–144.
[8] E. Furimsky, Appl. Catal. 6 (1983) 159.
[9] O.I. Senol, T.-R. Viljava, A.O.I. Krause, Catal. Today 100 (2005) 331.
[10] A.Y. Bunch, X. Wang, U.S. Ozkan, J. Mol. Catal. A: Chem. 270 (2007) 264.
[11] C. Song, Catal. Today 86 (2003) 211.
[12] S. Brunet, D. Mey, G. Pérot, C. Bouchy, F. Diehl, Appl. Catal. A: Gen. 278 (2005) 143.
[13] S. Kasztelan, H. Toulhoat, J. Grimblot, J.-P. Bonnelle, Appl. Catal. 13 (1984) 17.
[14] M. Badawi, L. Vivier, G. Pérot, D. Duprez, J. Mol. Catal. A: Chem. 293 (2008) 53.
[15] M. Badawi, L. Vivier, D. Duprez, J. Mol. Catal. A: Chem. 320 (2010) 34.
[16] J.-F. Paul, S. Cristol, E. Payen, Catal. Today 130 (2008) 139.
[17] M. Sun, J. Adjaye, A.E. Nelson, Appl. Catal. A: Gen. 263 (2004) 131.
[18] P. Raybaud, Appl. Catal. A: Gen. 322 (2007) 76.
[19] J.B. Binder, M.J. Gray, J.F. White, Z.C. Zhang, J.E. Holladay, Biomass Bioenergy 33 (2009) 1122.
[20] H. Pakdel, B. De Caumia, C. Roy, Biomass Bioenergy 3 (1992) 31.
[21] Q. Lu, Y. Zhang, Z. Tang, W. Li, X. Zhu, Fuel 89 (2010) 2096.
[22] E. Odebunmi, D. Ollis, J. Catal. 80 (1983) 56.
[23] B.S. Gevert, J. Otterstedt, F.E. Massoth, Appl. Catal. 31 (1987) 119.
[24] C. Aubert, R. Durand, P. Geneste, C. Moreau, J. Catal. 112 (1988) 12.
[25] E. Laurent, B. Delmon, Ind. Eng. Chem. Res. 32 (1993) 2516.
[26] B.S. Gevert, M. Eriksson, P. Eriksson, F.E. Massoth, Appl. Catal. A: Gen. 117 (1994) 151.
[27] T.-R. Viljava, R.S. Komulainem, A.O.I. Krause, Catal. Today 60 (2000) 83.
[28] F.E. Massoth, P. Politzer, M.C. Concha, J.S. Murray, J. Jakowski, J. Simons, J. Phys. Chem. B 110 (2006) 14283.
[29] O. I Senol, E.-M. Ryymin, T.-R. Viljava, A.O.I. Krause, J. Mol. Catal. A: Chem. 277 (2007) 107.
[30] Y. Romero, F. Richard, Y. Renème, S. Brunet, Appl. Catal. A: Gen. 353 (2009) 46.
[31] Y. Romero, F. Richard, S. Brunet, Appl. Catal. B: Environ. 98 (2010) 213.
[32] M. Badawi, S. Cristol, J.-F. Paul, E. Payen, C. R. Chim. 12 (2009) 754.
[33] E. Laurent, B. Delmon, J. Catal. 146 (1994) 281.
[34] E. Laurent, B. Delmon, App. Catal. 109 (1994).
[35] Y. Yoshimura, T. Sato, H. Shimada, N. Matsubayashi, A. Nishijima, Appl. Catal. 73 (1991) 55.
[36] C.N. Satterfield, C.M. Smith, Ind. Eng. Chem. Proc. Des. Dev. 24 (1985) 1000.
[37] G. Kresse, J. Hafner, Phys. Rev. B 47 (1993) 558.
[38] J.P. Perdew, J.A. Chevary, S.H. Vosko, K.A. Jackson, M.R. Pedersen, D.J. Singh, C. Frolais, Phys. Rev. B 46 (1992) 6671.
[39] G. Kresse, J. Joubert, Phys. Rev. B 59 (1999) 1758.
[40] S. Cristol, J.-F. Paul, E. Payen, D. Bougeard, S. Clemendot, F. Hutschka, J. Phys. Chem. B 104 (2000) 11220.
[41] S. Cristol, J.-F. Paul, E. Payen, D. Bougeard, S. Clemendot, F. Hutschka, J. Phys. Chem. B 106 (2002) 5659.
[42] D. Loffreda, Surf. Sci. 600 (2006) 2103.
[43] P.W. Atkins, Physical Chemistry, fifth ed., Oxford University Press, London, 1990.
[44] A. Travert, C. Dujardin, F. Mauge, E. Veilly, S. Cristol, J.F. Paul, E. Payen, J. Phys. Chem. B 110 (2006) 1261–1270.
[45] A. Travert, C. Dujardin, F. Maugé, S. Cristol, J.-F. Paul, E. Payen, D. Bougeard, Catal. Today 70 (2000) 255.
[46] W. Chen, PhD Thesis, RIPP (Beijing, China), University of Caen (France), 2009.
[47] S. Eijsbouts, J.J.L. Heinerman, H.J.W. Elzerman, Appl. Catal. A: Gen. 105 (1993) 53.
[48] P.J. Kooyman, J.A. Rob van Veen, Catal. Today 130 (2008) 135.
[49] P. Raybaud, J. Hafner, G. Kresse, S. Kasztelan, H. Toulhoat, J. Catal. 189 (2000) 129.
[50] J. Mijoin, V. Thévenin, N. Garcia Aguirre, H. Yuze, J. Wang, W.Z. Li, G. Pérot, J.L. Lemberton, Appl. Catal. A 180 (1999) 95.
[51] F. Bataille, J.L. Lemberton, P. Michaud, G. Pérot, M. Vrinat, M. Lemaire, E. Schulz, M. Breysse, S. Kasztelan, J. Catal. 191 (2000) 409.
[52] J.V. Lauritsen, S. Helveg, E. Laegsgaard, I. Stensgaard, B.S. Clausen, H. Topsøe, F. Besenbacher, J. Catal. 197 (2001) 1.
[53] J.V. Lauritsen, J. Kibsgaard, G.H. Olesen, P.G. Moses, B. Hinnemann, S. Helveg, J.K. Norskov, B.S. Clausen, H. Topsøe, E. Laegsgaard, F. Besenbacher, J. Catal. 249 (2007) 220.
[54] C. Dujardin, M.A. Lélias, J. van Gestel, A. Travert, J.C. Duchet, F. Maugé, Appl. Catal. A: Gen. 322 (2007) 46.
[55] H. Schweiger, P. Raybaud, H. Toulhoat, J. Catal. 212 (2002) 33.
[56] E. Krebs, B. Silvi, P. Raybaud, Catal. Today 130 (2008) 160.
[57] M. Egorova, R. Prins, J. Catal. 225 (2004) 417–427.
[58] J. van Gestel, C. Dujardin, F. Maugé, J.C. Duchet, J. Catal. 202 (2001) 78.